Functional renal imaging with ^{18}F-FDS PET in rat models of renal disorders

Rudolf A. Werner[1,2,3], Hiroshi Wakabayashi[1,4], Xinyu Chen[1,3], Mitsuru Hirano[1,3], Tetsuya Shinaji[1,3], Constantin Lapa[1], Steven P. Rowe[2], Mehrbod S. Javadi[2] and Takahiro Higuchi[1,3,5]

1. Department of Nuclear Medicine, University Hospital Würzburg, Würzburg, Germany;
2. Division of Nuclear Medicine and Molecular Imaging, The Russell H. Morgan Department of Radiology and Radiological Science, Johns Hopkins University School of Medicine, Baltimore, MD, United States;
3. Comprehensive Heart Failure Center, University Hospital Würzburg, Würzburg, Germany
4. Department of Nuclear Medicine, Kanazawa University, Kanazawa, Japan;
5. Department of Bio Medical Imaging, National Cerebral and Cardiovascular Research Center, Suita, Osaka, Japan.

Running title: ^{18}F-FDS in rat models of renal disorders

Word count: 4152

Address for Correspondence:
Takahiro Higuchi, M.D., Ph.D.
Department of Nuclear Medicine / Comprehensive Heart Failure Center, University Hospital Würzburg
Oberdürrbacher Strasse 6
97080 Würzburg, Germany
Phone: +49 931 201 35455; Fax: +49 931 201 6 444 00
E-mail: thiguchi@me.com

First author:
Rudolf A. Werner, MD, Resident
Division of Nuclear Medicine and Molecular Imaging,
The Russell H. Morgan Department of Radiology and Radiological Science,

Johns Hopkins University School of Medicine
601 N. Caroline St., JHOC 3230
Baltimore, MD, 21287, United States
Mail: werner_r1@ukw.de Phone: +1 443 430 4905

ABSTRACT

Background: Precise regional quantitative assessment of renal function is limited with conventional ^{99m}Tc-labeled renal radiotracers. A recent study reported that the positron emission tomography (PET) radiotracer 2-deoxy-2-^{18}F-fluorosorbitol (^{18}F-FDS) has ideal pharmacokinetics for functional renal imaging. Furthermore, ^{18}F-FDS is available via simple reduction from routinely used 2-deoxy-2-^{18}F-fluoro-D-glucose (^{18}F-FDG). We aimed to further investigate the potential of ^{18}F-FDS PET as a functional renal imaging agent using rat models of kidney diseases. **Methods:** Two different rat models of renal impairment were investigated: Glycerol induced acute renal failure (ARF) by intramuscular administration of glycerol in hind legs and unilateral ureteral obstruction (UUO) by ligation of the left ureter. 24h after these treatments, dynamic 30 min ^{18}F-FDS PET data were acquired using a dedicated small animal PET system. Urine ^{18}F-FDS radioactivity 30 min after radiotracer injection was measured together with co-injected ^{99m}Tc-diethylenetriaminepentaacetic acid (^{99m}Tc-DTPA) urine activity. **Results:** Dynamic PET imaging demonstrated rapid ^{18}F-FDS accumulation in the renal cortex and rapid radiotracer excretion via kidneys in control healthy rats. On the other hand, significantly delayed renal radiotracer uptake (continuous slow uptake) was observed in ARF rats and UUO-treated kidneys. Measured urine radiotracer concentrations of ^{18}F-FDS and ^{99}mTc-DTPA were well correlated ($R=0.84$, $P<0.05$). **Conclusions:** ^{18}F-FDS PET demonstrated favorable kinetics for functional renal imaging in rat models of kidney diseases. Advantages of high spatiotemporal resolution of PET imaging and simple tracer production could potentially complement or replace conventional renal scintigraphy in select cases and significantly improve the diagnostic performance of renal functional imaging.

KEYWORDS: ^{18}F-FDS; ^{99m}Tc-DTPA; PET; renal failure; unilateral ureteral obstruction; Glomerular filtration

INTRODUCTION

The best indicator of kidney function is considered to be the glomerular filtration rate (GFR). However, as the filtration process occurs simultaneously in millions of glomeruli, a direct measurement of GFR is not feasible (*1*). The filtered agent ^{99m}Tc-diethylenetriaminepentaacetic acid (^{99m}Tc-DTPA) is widely available as a means to determine split GFR estimation by plotting dynamic renogram time-activity curves from planar images. However, precise regional assessment of renal function is limited from this 2-dimensional approach. Furthermore, Compton scatter and soft tissue attenuation are major obstacles for reliable quantification. The use of hybrid imaging devices such as single-photon emission computed tomography/computed tomography enables 3-dimensional anatomic co-registration; however, prolonged single-photon emission computed tomography acquisition time and limited temporal resolution reduce the potential of dynamic imaging (*2*).

Dynamic tomographic imaging with positron emission tomography (PET) has intrinsic advantages of high temporal and spatial resolution when compared to the 2-dimensional planar approach employed with single photon imaging agents. Furthermore, as previously confirmed in an experimental study of healthy rats, the PET radiotracer 2-deoxy-2-^{18}F-fluorosorbitol (^{18}F-FDS) has emerged as a promising candidate for measuring renal function with high kidney extraction and excretion, low plasma protein binding, and high metabolic stability (*3*). Given the simple 1-step reduction of the most frequent PET radiotracer 2-deoxy-2-^{18}F-fluoro-D-glucose (^{18}F-FDG), the use of ^{18}F-FDS might open the window for clinical availability of renal PET imaging.

The purpose of the present study is to elucidate the imaging and kinetic characteristics of ^{18}F-FDS for the assessment of renal function in renal impaired rats by using models of acute renal failure (ARF) and unilateral ureteral obstruction (UUO).

MATERIALS and METHODS

Radiotracer Production

^{18}F-FDS was synthesized following a previously described procedure (*4*). In short, $NaBH_4$ (2 mg, 0.053 mmol) was added to a solution of ^{18}F-FDG in saline, and the resulting mixture was stirred at 35°C for 15 min. After quenching the reaction, the mixture was adjusted to a pH of 7.4 and filtered through an Alumina-N Sep-Pak cartridge (Waters, Eschborn, Germany). The filtrate was then reconstituted in saline and passed through a 0.22-µm Millipore filter into a sterile multi-dose vial. Radiochemical purity of >95% ^{18}F-FDS was confirmed by radio thin-layer chromatography (TLC; CR 35 Bio, Raytest, Straubenhardt, Germany) (80% acetonitrile with 20% water as eluent) (*3*).

DTPA kits (Fujifilm RI Pharma, Tokyo, Japan) were labelled using generator-produced ^{99m}Tc-pertechnetate according to the manufacturer's instructions.

Animal Preparation

Male Wistar rats weighing 200 - 250 g (n=18) were used. Experimental protocols were approved by the regional governmental commission of animal protection and conducted in strict performance according to the *Guide for the Care and Use of Laboratory Animals* published by the U.S. National Institutes of Health (National Institutes of Health publication 85-23, revised 1996) (*5*). ARF was induced by intramuscular injection of 50% glycerol (10mL/kg) in each hind leg after a 24 h water deprivation period (n=5) (6,7). 24 hours after glycerol injection, experimental tracer studies were conducted. UUO was induced by complete ligation of the left ureter near the renal pelvis (n=9) (8). 24 h after the ligation procedure, experimental studies were performed. As controls, experimental studies were also carried out in 4 control healthy rats.

Small Animal PET Imaging

Rats were studied with a high-resolution dedicated small animal PET system (Inveon micro PET, Siemens Healthcare, Erlangen, Germany) (9). Animals were maintained under anesthesia by 2% isoflurane during the entirety of the

experiments. ^{18}F-FDS was administered via the rat's tail vein (30 MBq) for PET imaging, ^{99m}Tc-DTPA (2 MBq) was co-injected for reference for urine gamma counting and autoradiography. The 30 min list-mode scan was started just before radiotracer injection. The list-mode data was sorted into 3-dimensional sinograms, which were then re-binned with a full 3-dimensional binning to reconstruct dynamic images using a 3-dimensional ordered subset expectation maximization method. The reconstructed dynamic images consisted of 56 acquired frames (15 frames × 8 sec, 26 frames × 30 sec, and 15 frames × 60 sec).

The obtained PET images were analyzed using an image-processing application (AMIDE Imaging software, version 1.0.1) (10). Three-dimensional regions of interests were manually drawn over the entire kidney including the medulla. The mean concentration of radioactivity within the regions of interests was expressed as the percentage of injected dose per tissue cubic centimeter (% ID/cm^3). Time-activity curves (renography) were generated, and the time points of maximal (T_{max}) and half-maximal concentration ($T_{1/2max}$) were computed.

Post-Mortem Analysis

For gamma counting, plasma was collected via tail artery during PET acquisition (10 min after tracer delivery). After PET acquisition (35 min after tracer injection), rats were euthanized, urine was collected by opening the abdominal cavity and autoradiography studies were conducted. Plasma and urine were counted for radioactivity in an automated gamma counter (Wizard, PerkinElmer, Waltham, MA). The radioactivity concentrations expressed as injected dose per gram (%ID/g) were calculated (*3*). Kidneys were frozen, and cut into 20 µm short axis slices using a cryostat (Leica, Nußloch, Germany). Dual-radiotracer autoradiography was performed to assess both ^{18}F-FDS and ^{99m}Tc-DTPA uptake. First, the imaging plate (Multi Sensitive Phosphor Screens, PerkinElmer, Shelton, CT) was exposed for 3 h to visualize the distribution of ^{18}F-FDS with a digital autoradiography system (CR 35 Bio, Raytest, Straubenhardt, Germany). After 18 h, to allow for the decay of ^{18}F, a second

exposure for 12 h was started to evaluate ^{99m}Tc-DTPA uptake. Following autoradiography, tissue slices were stained with hematoxylin and eosin.

Statistics

All results are displayed as mean ± standard deviation. The two-tailed paired Student's t-test was used to compare differences between two dependent groups, and the two-tailed independent Student's t-test for differences between independent groups. For correlative analyses, Pearson coefficients of correlation were calculated. A value of $P < 0.05$ was considered statistically significant. Statistical analysis was done with StatMate III (ATMS Co., Ltd.) and JMP (SAS Institute Inc., Cary, NC).

RESULTS

Small Animal Imaging

Whole body dynamic PET imaging demonstrated high renal radiotracer excretion via kidneys with low hepatobiliary clearance in control animals (Figs. 1 and 2). Blood flow through the inferior vena cava and arterial vasculature was visualized, followed by a gradual delineation of the renal cortex and transition of the activity into the collecting system/renal pelvis (Fig. 1A). Visual analysis demonstrated ^{18}F-FDS was solely excreted through the urinary system, and subsequently transited into the bladder. No obvious signal from other organs were detected (Fig. 1B). A normal renogram pattern, consistent with blood flow, parenchymal, and excretory phase with a T_{max} of 1.1 ± 0.6 min and $T_{1/2max}$ of 12.2 ± 3.0 min was derived in healthy control rats (Fig. 1C, top). As expected, the bladder demonstrated a continuous increase in controls (Fig. 1C, bottom).

In PET images of ARF rats, significantly reduced uptake in the renal cortex was identified compared to controls (Fig. 1A). Lower radiotracer excretion through the urinary system was observed. In particular, radiotracer transit to the bladder was delayed (Fig. 1B). These findings were further corroborated using

averaged radiotracer time-activity curves. The derived renograms showed a non-functioning pattern, indicating that glomerular filtration was impaired after glycerol injection (Fig. 1C, top). T_{max} was 0.5 ± 0.1 min in ARF rats ($p < 0.05$, vs. controls), whereas $T_{1/2max}$ was not reached during the scan of 30 min. Additionally, bladder activity was reduced and delayed in the ARF model (Fig. 1C, bottom).

In UUO rats, enlarged PET images of the renal area display a weak to moderate radiotracer retention in the renal cortex over time (Figure 2a). Lower and delayed uptake was observed on the obstructed side with no transition into the collecting system/renal pelvis (Fig. 2B, left kidney), whereas the contralateral side (Fig. 2B, right kidney) showed similar results to those obtained in control rats. Derived renograms demonstrated a typical pattern of an obstructed kidney: on averaged time-activity curves, the increase of activity of the obstructed side was very slow, with no further peak during the parenchymal phase and progressive parenchymal accumulation (Fig. 2C). For the UUO kidneys, T_{max} was 22.7 ± 4.5 min ($p < 0.0001$ vs. controls), whereas $T_{1/2max}$ was not reached.

Gamma Counting and Autoradiography Results

Radiotracer counting of co-injected ^{18}F-FDS and ^{99m}Tc-DTPA was performed in plasma (4 ARF rats, 4 controls) and urine (3 ARF rats, 3 controls). The ^{18}F-FDS concentrations in plasma (R=0.77) and urine (R=0.84) were well correlated with ^{99m}Tc-DTPA ($p<0.05$, Table 1). Autoradiography confirmed similar renal distribution of both radiotracers in healthy controls and ARF rats (Fig. 3). In regards to the hematoxylin and eosin staining, retained radioactivity was observed in the inner medullary collecting ducts.

In-Vivo Stability and Plasma Protein Binding

Radio-TLC analysis of rat plasma samples and ^{18}F-FDS solution revealed completely matched single spots in all samples from each group (n=2), indicating the non-existence of radiolabeled metabolites in blood 30 min after radiotracer administration. *In-vivo* serum protein binding of ^{18}F-FDS at 30 min

after radiotracer administration was quantified as minimal (<0.1%) by separation of free ^{18}F-FDS using ultrafiltration.

DISCUSSION

As the standard of renal function measurement, GFR assessment requires an exogenous marker that behaves similar to inulin, i.e. free filtration without any tubular secretion or absorption (*11*). Suitable exogenous markers for measuring renal function, such as ^{51}Cr-EDTA, are widely used in clinical practice and plasma clearance estimated by multiple blood samples increases its diagnostic accuracy, although repeated sampling makes it inconvenient (*11*). GFR estimation using ^{99m}Tc-DTPA planar imaging is biased by the applied method of scintigraphic GFR determination (*12*) and camera-based techniques depend on the precise assessment of renal depth for soft-tissue attenuation corrections (*13*). On the other hand, recent efforts have been made in the development of novel renal imaging agents focusing on tubular function and renal plasma flow instead of measuring GFR (*14,15*). With identical kinetics to the gold standard ^{131}I-orthoiodohippurate for measurement of effective renal plasma flow, ^{99m}Tc $(CO)_3$(fluoroethyl)iminodiacetic acid (^{99m}Tc$(CO)_3$FEDA) inherits the advantage of improved background activity correction; however, none of the current available methodolgy in place is able to solve this issue successfully (*16,17*). In contradistinction, as previously demonstrated in healthy rats and confirmed in the present study, ^{18}F-FDS allows for almost complete elimination of background activity from surrounding organs (*3*). We observed rapid excretion via the urinary system without visualized hepatobiliary clearance and high *in-vivo* stability along with low serum protein binding. Furthermore, in two different rat models of kidney diseases, functional impairment of the injured kidneys were successfully identified: In ARF rats radiotracer extraction by and excretion through both kidneys was low and minimal radiotracer accumulation in the bladder was observed. Imaging derived renograms showed a bilateral non-functioning pattern. In the UUO rat model, radiotracer extraction from the blood pool was reduced and transit from cortex to collecting system in the obstructed

kidney was significantly impaired. Renograms demonstrated a typical obstructed pattern on the affected side.

In a dual-tracer autoradiography study using the γ-camera imaging agent ^{99m}Tc-DTPA, biodistribution for both radiotracers yielded comparable findings. However, renal PET imaging offers numerous advantages, such as increased spatiotemporal resolution and accurate tomographic 3D quantitative capability (*17*). As a competitor for PET renal imaging, ^{68}Ga-EDTA has been recently introduced as a substitute for ^{99m}Tc-DTPA (*18*). Compared to its ^{68}Ga-labelled counterpart, ^{18}F-FDS provides a cost-effective approach of radiotracer production by a simple one-step reduction of ^{18}F-FDG, and its longer half-life allows for flexibility in study design. Further, it possesses the inherent advantages of lower positron energy along with higher positron yield. Strikingly, as an analog of sorbitol, its kinetic properties are theoretically identical to the ”gold standard“ inulin (sorbitol–to–inulin clearance ratio = 1.01) (*19*). However, regardless of the used radiotracer, the major obstacles of using renal PET imaging in a human setting have to been addressed, i.e. that current PET cameras do not allow to image the entire urinary system in a single field of view (*18*). Hence, costly large field whole body PET devices might be necessary to overcome this limitation or multiple PET and CT acquisitions would be required, which might hamper diagnostic accuracy.

In light of radiation exposure and higher costs, it remains a matter of debate in which clinical situation the use of PET/CT in renal radionuclide imaging would be most justified. A decade ago, renovascular hypertension or kidney transplant rejection were seen as major clinical renal PET indications; however, improvements in drug development and widespread availability of non-radiation methods such as ultrasound techniques have led to a massive decline of such study requests in recent years (*20-23*). Currently, common clinical indications include monitoring during chemotherapy or assessment of split renal function for various clinical indications, e.g. before radiotherapy or prior to live kidney donation (*24-26*). Based on the superior spatial and temporal resolution of PET, ^{18}F-FDS could potentially be applied in those clinical situations, especially for determining differential glomerular filtration.

Due to the promising results of recently published randomized clinical trials, treatment of inoperable, metastasized neuroendocrine tumors with radiolobaled somatotostatin analogues is currently gaining ground (*27*). However, renal irradiation from peptide receptor radionuclide therapy is most likely to be caused by cross-fire of radiolabeled somatostatin analogues from adjacent tubules and it was hypothetized that serial ^{99m}Tc-mercaptoacetyltriglycine studies might be a superior indicator for early stages of kidney dysfunction caused by endoradiotherapy (*28*). However, measurement of tubular extraction rate was unsuitable as an early diagnostic approach to identify an increased probability of later renal failure (*29*). Hence, a dual-radiotracer approach of somatostatin receptor PET together with ^{18}F-FDS PET could be potentially applied in patients scheduled for peptide receptor radionuclide therapy and replace common renography studies in the long-term.

Most importantly, creatinine clearance-based estimates of GFR are often used in pediatrics. However, changes in body mass limit the reliability of this method and accuracy is hampered in children with renal and urological disorders (*17*). Moreover, children can also have renal anatomic abnormalities, such as ureteropelvic junction obstruction (*30*). Ideally, when faced with these difficult clinical situations, ^{18}F-FDS renal PET might set the scene for effective decision making, as it provides simultaneous information about anatomic conditions along with functional significance of an obstruction (*17*). Given the increased count rates obtained with ^{18}F-FDS PET as compared to conventional imaging agents such as ^{99m}Tc-DTPA, a much lower activity of ^{18}F can be administered. Hence, mainly due to the advantages of PET over single-photon emission computed tomography, ^{18}F-FDS could potentially minimize radiation exposure in children without sacrificing image quality. Moreover, while performing a PET/CT study, the additional exposure of the CT component should be also considered. However, an (ultra)low dose CT along with the narrow field-of-view necessary for renal imaging could further lower radiation exposure to less than 0.25 mSv (*2*).

CONCLUSION

In two rat models of kidney disease, ^{18}F-FDS PET demonstrated favorable kinetics for functional renal imaging. Renal PET/CT has the potential to provide improved spatial and temporal functional data in clinical situations where relevant information cannot be easily obtained by other common non-invasive techniques. Due to its superior diagnostic performance and simple production via reduction of ^{18}F-FDG, ^{18}F-FDS might meet this urgent need in renal radionuclide imaging. Strikingly, ^{18}F-FDS could potentially minimize radiation exposure in children without sacrificing image quality. Further confirmatory studies in human are warranted.

ACKNOWLEDGMENTS

This work was supported by the Competence Network of Heart Failure funded by the Integrated Research and Treatment Center (IFB) of the Federal Ministry of Education and Research (BMBF) and German Research Council (DFG grant HI 1789/3-3). This project has received funding from the European Union's Horizon 2020 research and innovation programme under the Marie Sklodowska-Curie grant agreement No 701983. HW has received a JSPS Grant-in-Aid for Research (17K10353). No other potential conflicts of interest relevant to this article were reported.

This research was originally published in JNM. Rudolf A. Werner, Hiroshi Wakabayashi, Xinyu Chen, Mitsuru Hirano, Tetsuya Shinaji, Constantin Lapa, Steven P. Rowe, Mehrbod S. Javadi and Takahiro Higuchi. Functional renal imaging with ^{18}F-FDS PET in rat models of renal disorders. J Nucl Med. May 1, 2018;vol. 59 no. 5: 828-832.

REFERENCES

1. Soveri I, Berg UB, Bjork J, et al. Measuring GFR: a systematic review. *Am J Kidney Dis.* 2014;64:411-424.

2. Hofman MS, Hicks RJ. Gallium-68 EDTA PET/CT for renal imaging. *Semin Nucl Med.* 2016;46:448-461.

3. Wakabayashi H, Werner RA, Hayakawa N, et al. Initial preclinical evaluation of 18F-Fluorodeoxysorbitol PET as a novel functional renal imaging agent. *J Nucl Med.* 2016;57:1625-1628.

4. Li ZB, Wu Z, Cao Q, et al. The synthesis of 18F-FDS and its potential application in molecular imaging. *Mol Imaging Biol.* 2008;10:92-98.

5. Guide for the care and use of laboratory animals. *Bethesda, MD: National Institutes of Health; NIH publication 85-23.* 1985.

6. Singh AP, Junemann A, Muthuraman A, et al. Animal models of acute renal failure. *Pharmacol Rep.* 2012;64:31-44.

7. Westenfelder C, Arevalo GJ, Crawford PW, et al. Renal tubular function in glycerol-induced acute renal failure. *Kidney Int.* 1980;18:432-444.

8. Tantawy MN, Jiang R, Wang F, et al. Assessment of renal function in mice with unilateral ureteral obstruction using 99mTc-MAG3 dynamic scintigraphy. *BMC Nephrol.* 2012;13:168.

9. Disselhorst JA, Brom M, Laverman P, et al. Image-quality assessment for several positron emitters using the NEMA NU 4-2008 standards in the Siemens Inveon small-animal PET scanner. *J Nucl Med.* 2010;51:610-617.

10. Loening AM, Gambhir SS. AMIDE: a free software tool for multimodality medical image analysis. *Mol Imaging.* 2003;2:131-137.

11. Gaspari F, Perico N, Remuzzi G. Measurement of glomerular filtration rate. *Kidney Int Suppl.* 1997;63:S151-154.

12. Mulligan JS, Blue PW, Hasbargen JA. Methods for measuring GFR with technetium-99m-DTPA: an analysis of several common methods. *J Nucl Med.* 1990;31:1211-1219.

13. Taylor A, Lewis C, Giacometti A, Hall EC, Barefield KP. Improved formulas for the estimation of renal depth in adults. *J Nucl Med.* 1993;34:1766-1769.

14. Lipowska M, Klenc J, Jarkas N, Marzilli LG, Taylor AT. Monoanionic 99mTc-tricarbonyl-aminopolycarboxylate complexes with uncharged pendant groups: radiosynthesis and evaluation as potential renal tubular tracers. *Nucl Med Biol.* 2017;47:48-55.

15. Klenc J, Lipowska M, Taylor AT. Synthesis and evaluation of 99mTc(CO)3 (FEDA): a new dual-purpose 99mTc/18F renal imaging agent. *J Nucl Med.* 2015;56:654.

16. Blaufox MD. Renal background correction and measurement of split renal function: The challenge. *Eur J Nucl Med Mol Imaging.* 2016;43:548-549.

17. Blaufox MD. PET measurement of renal glomerular filtration rate: Is there a role in nuclear medicine? *J Nucl Med.* 2016;57:1495-1496.

18. Hofman M, Binns D, Johnston V, et al. 68Ga-EDTA PET/CT imaging and plasma clearance for glomerular filtration rate quantification: comparison to conventional 51Cr-EDTA. *J Nucl Med.* 2015;56:405-409.

19. Willie W, Smith HF, Smith HW. Renal excretion of hexitols (sorbitol, mannitol, and dulcitol) and their derivatives (sorbitan, isomannide, and sorbide)

and of endogenous creatinine-like chromogen in dog and man. *J Biol Chem.* 1940;135:231-250.

20. Szabo Z, Xia J, Mathews WB, Brown PR. Future direction of renal positron emission tomography. *Semin Nucl Med.* 2006;36:36-50.

21. Taylor AT. Radionuclides in nephrourology, Part 2: pitfalls and diagnostic applications. *J Nucl Med.* 2014;55:786-798.

22. Textor SC. Current approaches to renovascular hypertension. *Med Clin North Am.* 2009;93:717-732, Table of Contents.

23. Hanssen O, Erpicum P, Lovinfosse P, et al. Non-invasive approaches in the diagnosis of acute rejection in kidney transplant recipients. Part I. In vivo imaging methods. *Clin Kidney J.* 2017;10:97-105.

24. Delbeke D, Segall GM. Status of and trends in nuclear medicine in the United States. *J Nucl Med.* 2011;52 Suppl 2:24S-28S.

25. Jackson P, Foroudi F, Pham D, et al. Short communication: timeline of radiation-induced kidney function loss after stereotactic ablative body radiotherapy of renal cell carcinoma as evaluated by serial (99m)Tc-DMSA SPECT/CT. *Radiat Oncol.* 2014;9:253.

26. Hartlev LB, Boeje CR, Bluhme H, Palshof T, Rehling M. Monitoring renal function during chemotherapy. *Eur J Nucl Med Mol Imaging.* 2012;39:1478-1482.

27. Strosberg J, El-Haddad G, Wolin E, et al. Phase 3 trial of 177Lu-Dotatate for midgut neuroendocrine tumors. *N Engl J Med.* 2017;376:125-135.

28. Sabet A, Ezziddin K, Pape UF, et al. Accurate assessment of long-term nephrotoxicity after peptide receptor radionuclide therapy with (177)Lu-

octreotate. *Eur J Nucl Med Mol Imaging.* 2014;41:505-510.

29. Werner RA, Beykan S, Higuchi T, et al. The impact of 177Lu-octreotide therapy on 99mTc-MAG3 clearance is not predictive for late nephropathy. *Oncotarget.* 2016;7:41233-41241.

30. Williams B, Tareen B, Resnick MI. Pathophysiology and treatment of ureteropelvic junction obstruction. *Curr Urol Rep.* 2007;8:111-117.

FIGURES

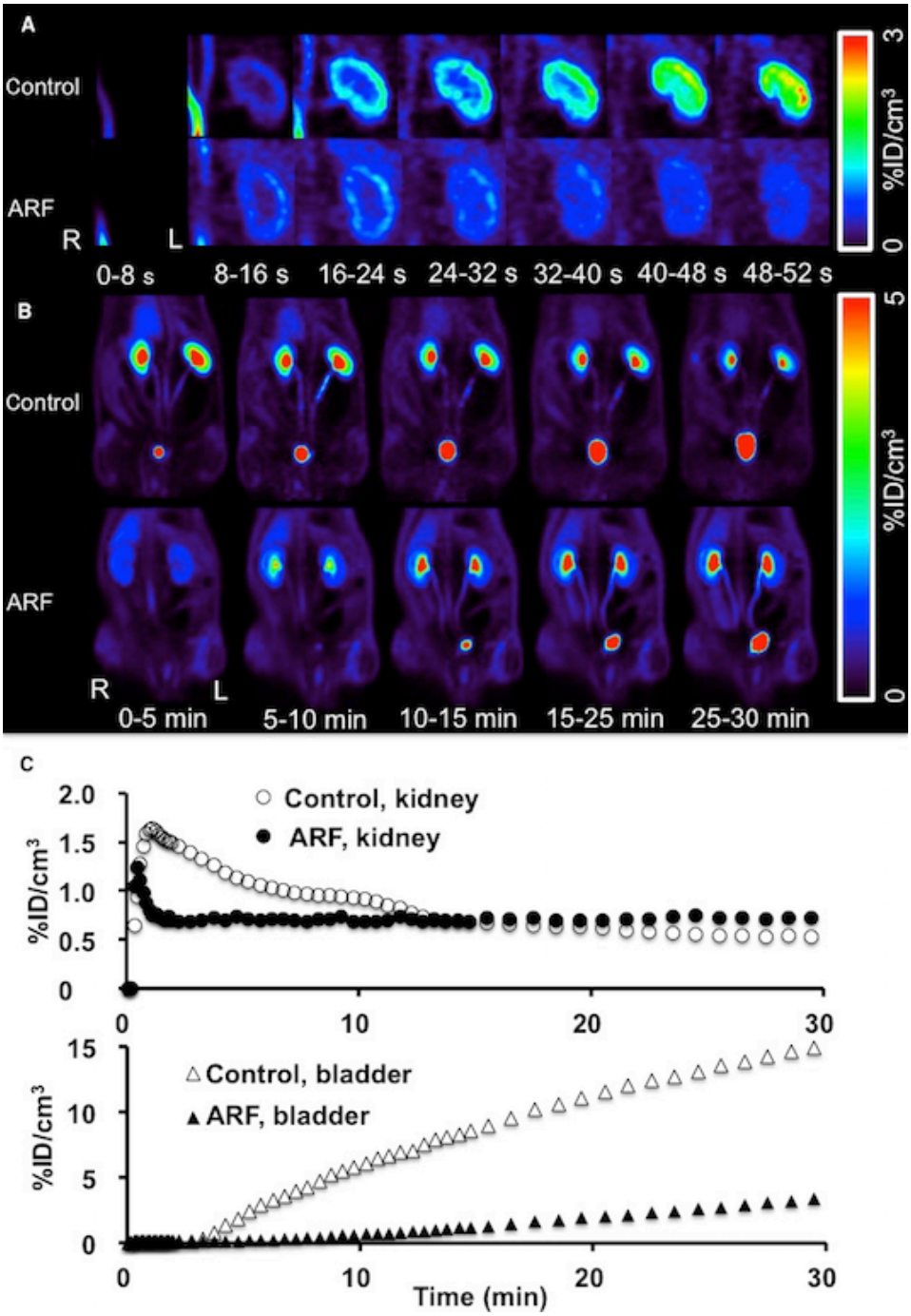

Figure 1. ***In-vivo*** **^{18}F-FDS PET imaging in controls and ARF rats. (a)** Dynamic left kidney images of coronal views. Rapid tracer accumulation in the renal cortex can be observed in control rat. In contrast, reduced renal tracer uptake in the renal cortex is shown in ARF rat. **(b)** Whole body dynamic PET images in coronal views. High tracer secretion exclusively via the kidneys and

time dependent increase of bladder activity are seen in control rats, reduced renal tracer secretion via the kidneys and delayed increase of bladder activity are observed in ARF rats. **(c)** Average time-activity curves of the kidneys (top) and bladder (bottom) obtained by dynamic PET imaging (averaged T_{max} of the kidneys in ARF rats: 0.5 ± 0.1 min). Low tracer secretion via the kidneys is observed in the ARF rat model. R=right, L=left, %ID=percentage injected dose.

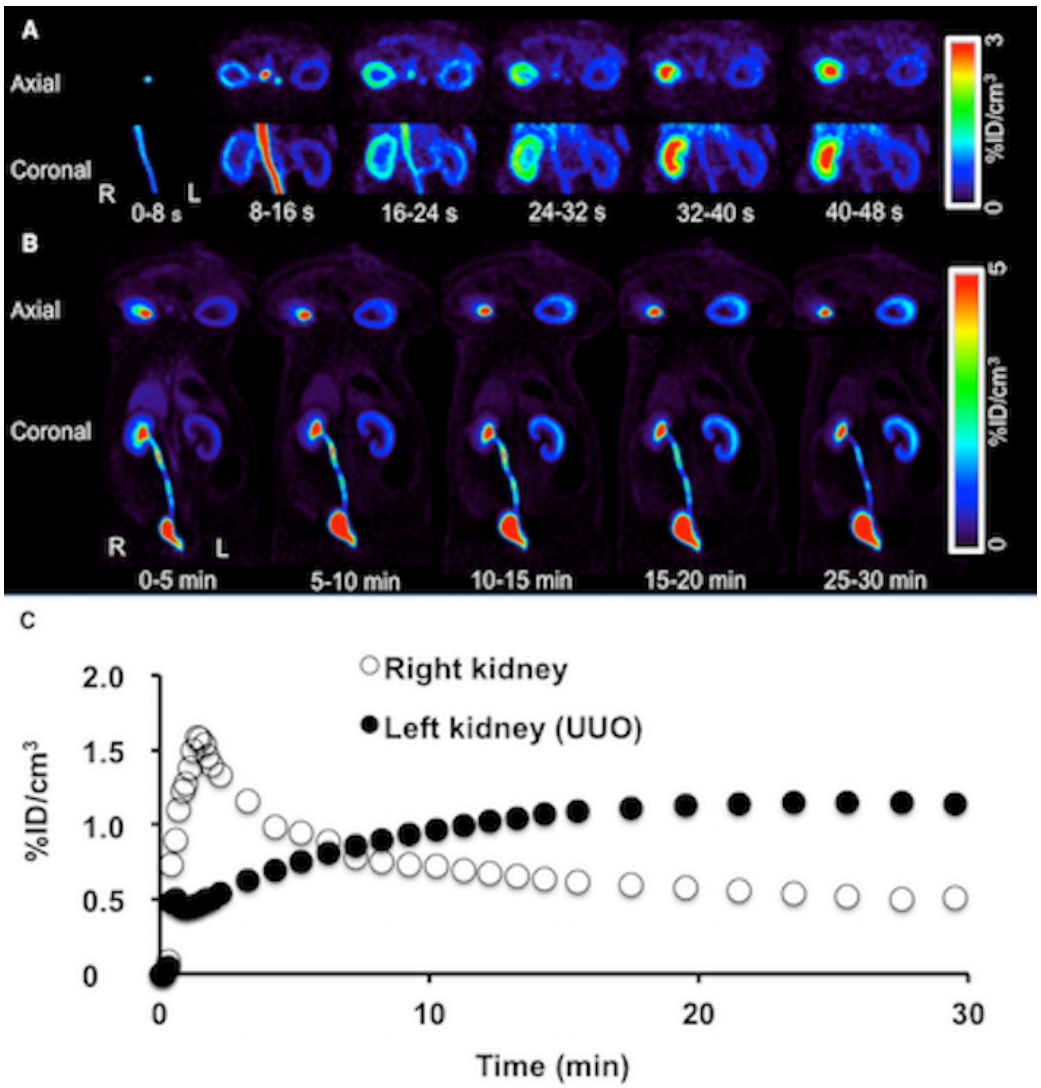

Figure 2. ***In-vivo*** **^{18}F-FDS PET imaging in UOO rats. (a)** Dynamic kidney images of axial and coronal views. Reduced renal tracer uptake in the renal cortex is shown in the affected kidney. On the other hand, rapid tracer accumulation in the renal cortex can be observed in the contralateral kidney. **(b)** Whole body dynamic PET images in axial and coronal views. The excretion of ^{18}F-FDS to renal pelvis is not observed in UUO kidney, while ^{18}F-FDS gets into renal pelvis in the contralateral kidney at 0-5 min. Time dependent increase of the UUO kidney uptake is seen. **(c)** Average time-activity curves of the kidneys obtained by dynamic PET imaging (averaged T_{max} of the kidneys in UUO rats: 22.7 ± 4.5 min). Tracer deposition in the cortex is observed in the UUO kidney. R=right, L=left, %ID=percentage injected dose.

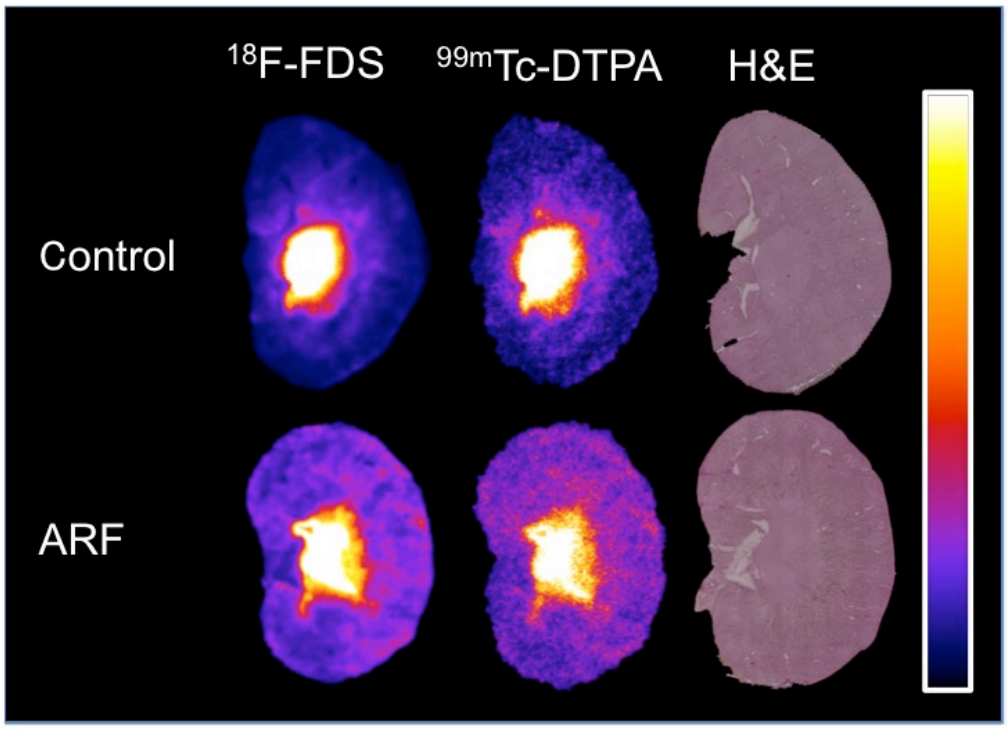

Figure 3. Coronal axis slices of the dual-tracer autoradiography study using ^{18}F-FDS and ^{99m}Tc-DTPA in healthy controls and in ARF rats. Tracer distribution of ^{18}F-FDS and ^{99m}Tc-DTPA showed comparable patterns in both controls and ARF rats. High radioactivity was observed in the inner medulla of the kidney referring to hematoxylin and eosin (H&E) staining.

TABLE

	^{18}F-FDS (%ID/g)	^{99m}Tc-DTPA (%ID/g)
Plasma	0.16	1.15
	0.15	0.43
	0.21	0.25
	0.3	0.89
	0.7	1.22
	0.4	1.35
	0.5	1.62
	0.72	2.23
Urine	6.8	20.9
	2.3	6.2
	4.4	4.6
	1.7	5.7
	1.4	3.8
	2.7	4.8

Table 1. Measured plasma and urine concentrations for radiotracer counting studies of co-injected ^{18}F-FDS and ^{99m}Tc-DTPA (plasma, 4 ARF rats and 4 controls as well as for urine, 3 ARF rats and 3 controls). The ^{18}F-FDS concentrations derived from plasma (R=0.77) and urine (R=0.84) were correlated with ^{99m}Tc-DTPA ($p<0.05$, each). %ID=percentage injected dose per gram.